Diyala Journal of Engineering Sciences

Journal homepage: https://djes.info/index.php/djes

ISSN: 1999-8716 (Print); 2616-6909 (Online)

Numerical Assessment of Pipeline Damage Due to an External Circumferential Semi-Elliptical Crack

Mohammed Amine Khater[1*], Chaaban Aroussi[2], Elamine Abdelouahed[3], Bassam Gamal Nasser Muthanna[4], Mohamed Mokhtari[1], Habib Benzaama[1]

[1] LaRTFM Laboratory, Mechanical Engineering Department, National Polytechnic School of Oran Maurice Audin, Oran, 31000, Algeria.
[2] LPTPM Laboratory, Mechanical Engineering Departement, Faculty of Technology, Hassiba BenBouali University of Chlef, Chlef, 02000, Algeria.
[3] LABAB Laboratory, Mechanical Engineering Department, National Polytechnic School of Oran Maurice Audin, Oran, 31000, Algeria.
[4] Department of Mechatronics Engineering, Faculty of Engineering and Computing, University of Science and Technology, Aden, Yemen.

ARTICLE INFO

Article history:
Received: 28/07/2025.
Revised: 27/09/2025.
Accepted: 27/10/2025.
Available online: 10/12/2025.

Keywords:
Pipeline integrity,
Semi-elliptical crack,
Abaqus,
Extended Finite Element Method (XFEM),
Numerical assessment,

ABSTRACT

This paper presents a numerical evaluation of pipeline damage caused by an external circumferential semi-elliptical crack. The study utilizes the Abaqus software and the Extended Finite Element Method (XFEM) to model and analyze the crack behavior. Various parameters such as crack size, internal pressure, and loading conditions are investigated to assess their influence on pipeline integrity. The results reveal that as internal pressure increases from 300 to 600 bar, the pipe's bearing capacity significantly decreases due to heightened stress concentrations around crack tips, leading to increased hoop stress and Stress Intensity Factors (SIFs), which accelerate crack propagation. Higher pressures also promote crack nucleation and growth, further reducing the effective cross-sectional area and weakening the pipe's load-carrying ability. Additionally, the analysis highlights the critical influence of defect size (a/t ratio) on stress distribution and residual strength: as the a/t ratio increases, the pipe becomes more vulnerable to failure at lower stress levels. The critical crack size is identified at the intersection of the resistance curve and the ultimate stress line, beyond which failure occurs before reaching the material's full strength. Non-physical regions, where resistance exceeds ultimate stress, are disregarded to ensure realistic defect assessments. Under an internal pressure of 30 MPa, pipes with a/t ratios of 0.50 and 0.62 remain within the safety zone, while those with a/t ratios of 0.75 and 0.80 enter the failure zone, indicating a substantial loss of structural integrity and an increased risk of fracture.

1. INTRODUCTION

Pipelines are critical infrastructure systems used to transport oil, gas, and water across long distances. Ensuring their structural integrity is essential to prevent catastrophic failures that may cause environmental damage, loss of life, and economic disruption [1]. Among the various defects that threaten pipeline safety, circumferential semi-elliptical cracks are of particular concern due to their tendency to propagate rapidly under operational loads. Typically originating on the external surface, these cracks are characterized by their semi-elliptical geometry, which varies in size and orientation, and can significantly compromise structural stability [2–4].

Numerous studies have applied experimental, analytical, and numerical methods to assess pipeline integrity [5–9]. In particular, numerical modeling using the Extended Finite Element Method (XFEM) has proven effective for simulating crack growth and evaluating failure mechanisms [10–15]. These simulations provide precise insights into crack propagation and its effects on pipeline performance, supporting informed decisions for maintenance

*Corresponding author's Email: medkhater@outlook.fr
DOI: 10.24237/djes.2025.18405

planning and risk mitigation [16]. However, most existing works have focused on simplified defect geometries or limited loading conditions, leaving a gap in understanding the behavior of external circumferential semi-elliptical cracks under combined effects of crack geometry, internal pressure, and applied loading.

The objective of this study is to investigate the structural response of pipelines containing circumferential semi-elliptical cracks using Abaqus and XFEM. By systematically varying crack dimensions, internal pressure, and loading conditions, the study aims to identify the key factors governing crack propagation and evaluate their impact on pipeline integrity. The findings are expected to improve the prediction of pipeline failure and support the development of more effective maintenance and risk management strategies.

2. BACKGROUND AND SIGNIFICANCE

The Extended Finite Element Method (XFEM) is a robust numerical approach for modeling crack propagation in complex geometries without requiring mesh alignment along crack paths [17]. By incorporating enrichment functions to represent the discontinuities introduced by crack surfaces [18], XFEM extends the conventional Finite Element Method (FEM). This enables accurate simulation of crack behavior in structures subjected to diverse loading conditions, such as pipelines.

In XFEM, the displacement field is locally enriched in the vicinity of the crack tip to accurately capture crack propagation. This is accomplished by augmenting the standard shape functions with additional terms that represent the singular stress field near the crack tip [19]. Consequently, XFEM formulations enable the simulation of crack growth without the need for remeshing, making the method particularly suitable for modeling crack propagation in pipelines subjected to structural degradation caused by corrosion, fatigue, or other factors [17], [20].

Several studies have demonstrated the effectiveness of XFEM in modeling crack propagation in pipelines and other engineering structures. For instance, the authors of [10] employed XFEM to analyze crack growth in pipelines subjected to cyclic loading, while [21] investigated the fatigue crack growth behavior in pipelines through XFEM simulations. Similarly, [22] examined the influence of cyclic loading frequency on the fatigue crack growth behavior of pipeline steel using XFEM-based approaches.

By leveraging XFEM, researchers can accurately predict crack propagation and assess its implications for pipeline integrity under various operating conditions. This enables informed decision-making regarding maintenance and risk mitigation strategies to ensure the safe and reliable operation of pipelines.

Table 1. Comparison between FEM and XFEM

Traditional FEM	XFEM
Requires remeshing when crack grows or changes geometry	Captures crack initiation and propagation without remeshing
Fine mesh needed around the crack tip	Standard mesh sufficient; enrichment functions capture singularities
Depends heavily on mesh refinement	Higher accuracy with enrichment functions, even with coarser meshes
Difficult to simulate arbitrary crack growth	Handles complex crack growth paths automatically
Challenging for semi-elliptical and evolving cracks	Well-suited for semi-elliptical cracks and crack propagation in pipelines

In Abaqus, the Extended Finite Element Method (XFEM) was employed to model crack initiation and propagation. The displacement-based geometric enrichment option was selected to capture the discontinuity along the crack path. Each enriched element was integrated using a full Gauss integration scheme with 4 × 4 Gauss points to ensure accuracy near the crack front. Crack initiation was governed by the Maximum Principal Stress (MAXPS) criterion, with failure occurring once the maximum principal stress exceeded the material's tensile strength. Crack propagation followed the default damage evolution law based on energy release rate, and the direction of propagation was determined by the local maximum principal stress criterion.

3. GEOMETRICAL MODEL

The pipeline geometry, including the semi-elliptical crack, was modeled using the pre-processing module of Abaqus. A refined mesh was employed in the vicinity of the crack tip to ensure accurate representation of the stress field and subsequent crack propagation behavior.

The geometrical model of the 85/8-inch pipeline is constructed using appropriate dimensions (D=219.1 mm and t=15.9 mm).

Table 2. Mechanical properties of the API 5L X80 pipe [23].

Grade	Yield strength	Ultimate tensile strength	Poisson's ration	Elastic modulus
X80	641 MPa	753 MPa	0.3	210 GPa

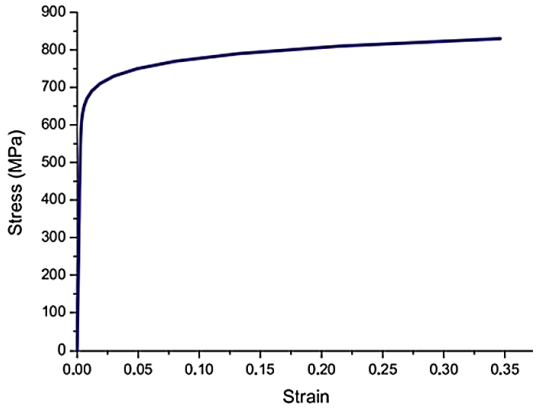

Figure 1. True stress-strain curve of X80 steel.

The surface (25/8; 50/10; 100/12) crack was introduced on the external surface of the pipe and defined as a semi-elliptical flaw with depth and surface length 2c. The initial aspect ratio (a/c) was set to 8/25, and the crack front was generated using an elliptical arc. During the XFEM analysis, the crack front was allowed to evolve naturally according to the propagation criterion, and thus the initial a/c ratio was not constrained but evolved as dictated by the stress field. In this study, a semi-elliptical crack size is varied to consider different case studies. The material properties of API 5L X80 have been shown in Table 2 and Figure 1. Figure 2 illustrated the geometrical model.

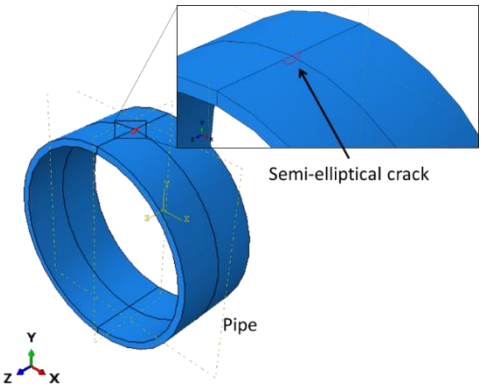

Figure 2. Geometrical model & crack emplacement.

4. NUMERICAL MODELING

Boundary conditions were applied by fully constraining both pipe ends (all translational and rotational degrees of freedom), while internal pressure was applied as a uniform surface load on the internal wall. This setup reflects conservative loading conditions, as it prevents end displacements and forces the pipe wall to carry the full pressure-induced stresses. In each simulation, the pressure was applied incrementally in Abaqus/Standard until the target magnitude was reached, allowing the nonlinear response and potential crack propagation to be captured. These conditions are chosen to represent realistic scenarios based on operational data and industry standards. Figure 3 showed the boundary condition of pipe.

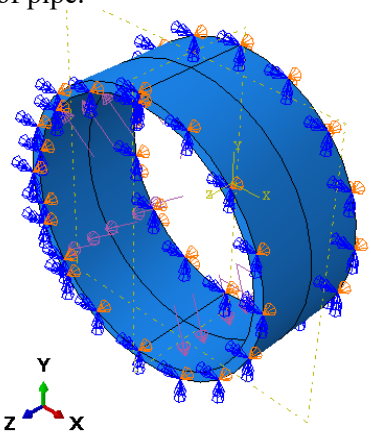

Figure 3. Loading and boundary conditions of geometrical model.

The crack is introduced at the specified location on the pipeline surface, and its propagation under applied loading is simulated using XFEM. Crack growth is governed by criteria such as stress intensity factors and energy release rates, which determine both the direction and rate of propagation.

The finite element simulations were carried out in Abaqus/Standard using the Extended Finite Element Method (XFEM) framework to model the semi-elliptical surface cracks without requiring remeshing during crack initiation. The pipe was modeled using 3D 8-node linear brick elements with reduced integration (C3D8R), which are well suited for capturing stress gradients around defects. To improve accuracy in the crack front region, a local mesh refinement strategy was employed, with the smallest element size near the crack front being approximately 1.0 mm, gradually coarsening toward the far-field regions. A mesh convergence study was performed to ensure that the displacement and load capacity results were insensitive to further refinement. Figure 4 showed the overview of mesh of structure.

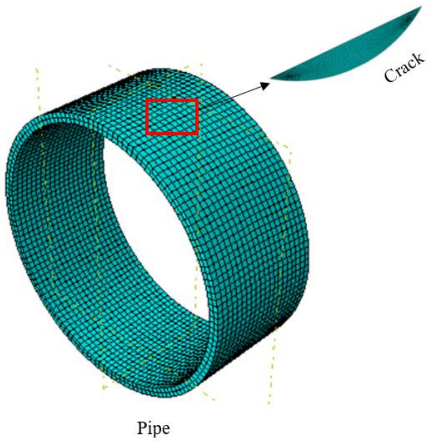

Figure 4. Overview of mesh structure.

Mesh refinement near the crack tip was performed to capture the stress singularity and ensure accurate

crack propagation modeling. Different mesh densities were tested, and convergence was assessed based on stress distribution and crack growth behavior. The final mesh was selected to balance accuracy and computational cost, as summarized in Table 3.

Table 3. Mesh Convergence Results

Number of elements	Max Von Mises stress (MPa)
5753	4415
5867	4420
7342	4421
10906	4421

5. RESULTS AND DISCUSSION

5.1 Internal pressure loading

The internal pressure dependence of the bearing capacity for a pipe with a semi elliptic crack is shown in Figure 5. As can be seen from this figure, with an increase in internal pressure from 300 to 600 bar, the bearing capacity of the pipe decreases. Such behavior could be interpreted by the increase in the stress concentration at the site of the defect, in particular around the tips of the crack. The hoop stress increases with the increase in pressure, and consequently, the SIF at the crack tips increases, which causes acceleration in the crack propagation. It can also be seen from the figure that at increased pressures, nucleation of cracks decreases the effective cross-sectional area carrying the load, and hence the capacity of the pipe to bear the external loads decreases drastically. The image also shows that at high values of pressure; localized plastic deformation may develop around the crack tip further weakening the structure. The overall trend of the image is that, within the range from 300 to 600 bar of internal pressure, the defect has become more critical; this corresponds to a reduced carrying capacity and loss of structural integrity in service.

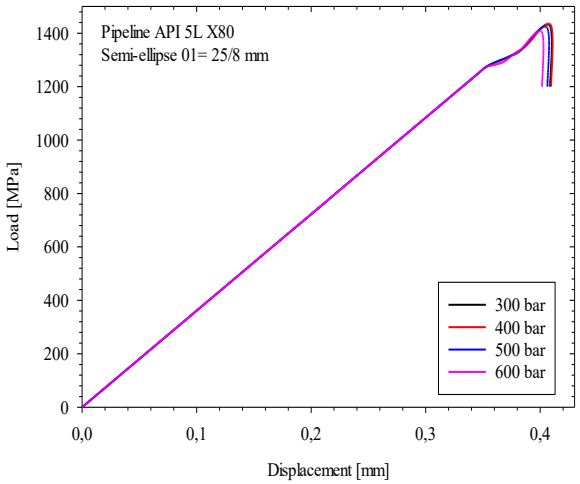

Figure 5. load-displacement curve for defect a/t=0.50.

Figure 6 presents the distribution of Von Mises stress in a pipe with a semi-elliptical crack measuring 25/8 mm, under different internal pressures. There is an increase in the level of stress concentration around crack tips as the internal pressure increases from 300 to 600 bar. This may be realized from the increased magnitude of the value of stress around the defect regions, hence showing the possibility of yielding or plastic deformation. The distribution of the Von Mises stresses indicates that the increment in the value of internal pressure increases the value of the stress state around the defect, which is the possibility of crack growth and the loss of the carrying capacity of the structure. The contour of stress has been expanded at a higher value of pressure, and the impact of fracture on the structural integrity of the pipe is large, leading to accelerating material failure. It succeeds in illustrating the behavior of the stress field while pressure increases and, more importantly, in pointing out that the important role of pressure in the weakening of structures goes along with the increased possibility of damage near the defect.

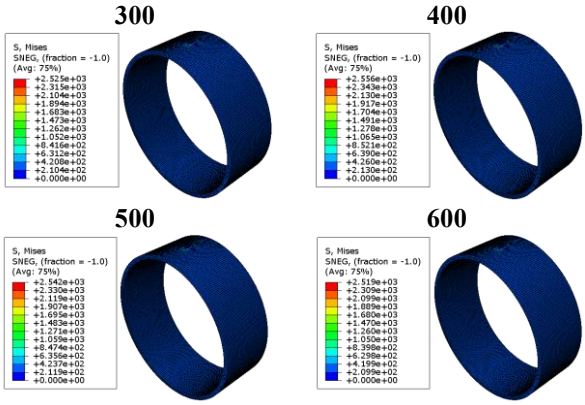

Figure 6. Von misses stress distribution at different pressure for defect a/t=0.50In.

Figure 7, the impact of internal pressure on the bearing capacity of the pipe containing a larger semi-elliptical crack (50/10 mm) is presented. As the internal pressure increases from 300 to 600 bar, the figure shows a more rapid decline in bearing capacity compared to the smaller crack case. A larger semi-elliptical crack may weaken the structural behavior of the pipe more than a crack with a size of 25/8 mm for internal pressures of 300, 400, 500, and 600 bar. Indeed, the increased size in the cracks provides a bigger area that can favor stress concentration. Hence, it is expected that for each level of pressure, SIFs at the crack tip are higher than those for the smaller-sized defect.

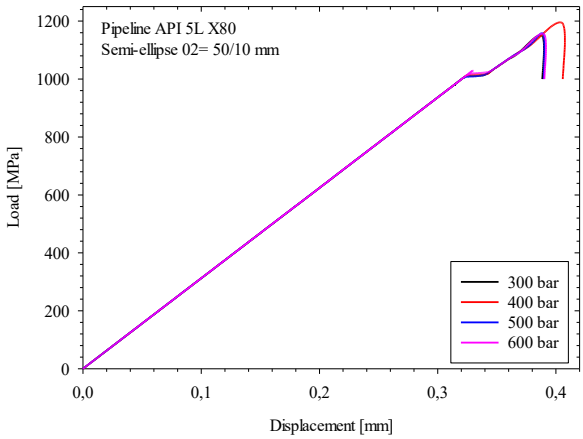

Figure 7. load-displacement curve for defect a/t=0.62.

At 300 bar, load-carrying capacity is still provided by the pipe, although substantially smaller because of the larger crack. By further increase in pressure to 400, 500 and 600 bar, stress intensity around crack tips starts to grow more highly nonlinear. Larger fracture allows for more pronounced crack opening and propagation, hence lowering the effective load-carrying area. The bearing capacity decreases much faster with internal pressure compared to the case of the smaller fracture. Furthermore, because of the bigger defect, it leads to early localized plastic deformation around the points of fracture during the loading phase, which further weakens the pipe.

In fact, with a pressure of 600 bar, there is a much greater danger of crack growth and possible failure. This is due to the larger semi elliptical fracture that has the capability to begin widening under a rapid pressure, greatly reducing both the load-carrying capacity and the general structural integrity of the pipe. That is, due to the more significant fracture size, the internal pressure increases cause faster decline of bearing capacity of the pipe, and much earlier, the defect turns out to be critical compared to the smaller crack.

Figure 8 shows the distribution of Von Mises stresses for the larger semi-elliptical crack of dimensions 50/10 mm at pressures of 300, 400, 500, and 600 bar. High stress concentration around the fracture is recorded compared to the smaller crack whose dimensions were 25/8 mm. This graph provides a comparison of how, for every pressure level, larger crack sizes shift the SIF at the crack tips upward, reflecting increased stress concentrations over an increased area. Even for 300 bar, the distribution of Von Mises stresses already reflects significant degradation of the load-carrying ability such that even at moderate pressure, the pipe is already structurally weak. For the same increase in pressure, accordingly to 400, 500, and 600 bar, it can be seen that there is a significant rise in the stress concentration around the fracture and that a larger stress field spreads from the defect zone. It further shows that the fracture opening has increased greatly, which may also be attributed to the much bigger amount of plastic deformation occurring at an earlier stage and being much more important in this case than in the case of a small crack. This thus reduces significantly the effective cross-sectional area of the pipe. The high-stress zones at 600 bar do hint that internal pressure may result in larger and quicker loss of load-carrying ability with larger sizes of cracks.

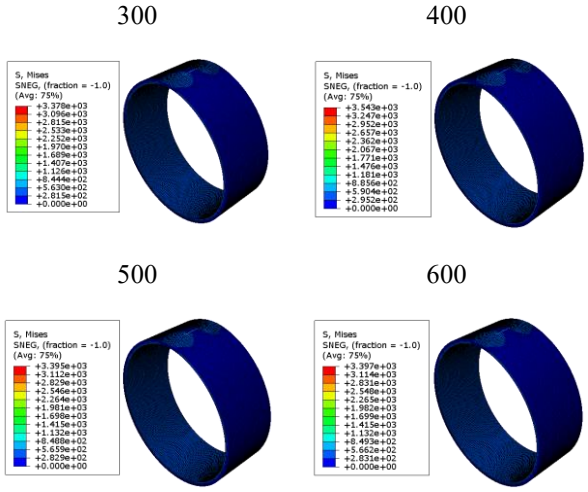

Figure 8. Von misses stress distribution at different pressure for defect a/t=0.62.

The internal-pressure-dependent bearing capacity of a pipe with the larger-sized semi-elliptical crack, 75/12 mm, is shown in Figure 9. As observable from this figure, for an increase in internal pressure-from 300 to 600 bar-the degradation in bearing capacity becomes rapid and serious, which is much more severe than what was experienced in previous cases dealing with smaller cracks due to the greater dimensions of the crack, near-tip stress concentrations are markedly greater, leading to much greater values for the stress intensity factors for all pressure levels. At 300 bar, bearing capacity is already considerably reduced with respect to smaller defects; the greater extension of the crack induces greater distribution of the stresses around the defect. While the pressure is increased to 400, 500, and 600 bar, respectively, the figure shows a significant decline in the load-carrying capacity of the pipe. The decline is because a larger fracture ensures higher speed of propagation and crack opening that drastically reduces the structural integrity of the pipe. It is also seen from the same figure that the localized plastic deformation develops much more strongly with increasing pressure-especially around the fracture points-further weakening the pipe. From the figure, it clearly follows that at an internal pressure of 600 bar, sudden failure due to the rapid growth of the defect and such an essential loss of carrying

capability is imminent. Figure 9 brings out that a larger semi-elliptical defect 75/12 mm results in a much quicker and more drastic fall in the load-carrying capability of the pipe with increasing internal pressure, the defect attaining critical status far in advance compared to what has been observed with smaller defects.

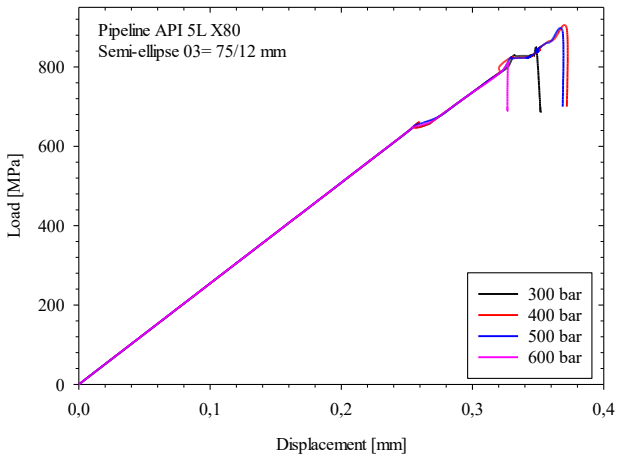

Figure 9. load-displacement curve for defect a/t=0.75.

Figure 10 shows the distribution of the Von Mises tension in the pipe with a greater semi elliptical crack (75/12 mm) for internal pressures from 300 to 600 bar. It is possible to observe that the concentration of tension in the defect region is more accentuated with regard to smaller situations of fracture. The image still shows that the scenario of 300 bar already has substantial tension around the fracture, indicating early compromise of structural integrity. It is observed that with higher pressure values of 400, 500, and up to 600 bar, the rise in stress concentrations and the area covered becomes very intense around the crack tips, with much larger SIFs.

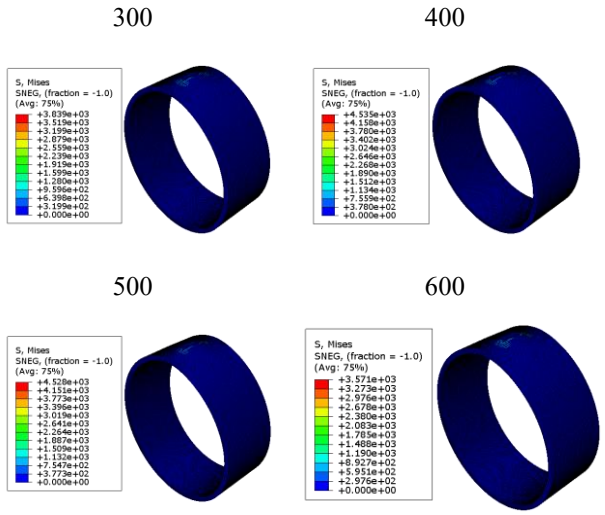

Figure 10. Von misses stress distribution at different pressure for defect a/t=0.75.

This figure also reveals that for higher pressures, localized plastic deformation is initiated earlier and develops more widely, since a larger fracture allows larger crack opening and propagation. At 600 bar, the distribution of the Von Mises stress indicates that a critical condition is reached, including an evident possibility of fast fracture propagation and an imminent failure under such conditions-representing more serious degradations in the structure than what was previously observed in crack cases.

Shown in Figure 11 is how internal pressure affects the bearing capacity of the pipe with an even larger semi-elliptical defect of 100/14 mm. This figure shows that with increased internal pressure from 300 to 600 bar, there occurs a dramatic and accelerated decline in bearing capacity that reflects the great influence of such a big crack size. The geometry of this defect provides a very significant stress concentration at the crack tips, hence the extremely high values of SIF for all pressure levels considered. Already at 300 bar, bearing capacity is severely reduced in comparison with the previous cases, since the larger defect entails a serious redistribution of the stresses throughout the pipe wall. The graph indicates that the trend is a steep and drastic fall in load-carrying capacity, starting from 400 to 500 and finally to 600 bar. Due to the increased size of a crack, greater and faster crack growth is produced which cause severe degradation in the structure, and the pipe will become highly susceptible to failure.

As seen from the figure, the plastic deformation around the crack tips is very extensive. There is a huge weakening of the material near the defect because of the increased pressure. Thus, at 600 bar, the pipe already approaches a failure threshold, as evidenced by the steep drop in bearing capacity-the defect reaches a critical state and seriously reflects on the stability of the structure. In general, Figure 11 emphasizes the fact that in the presence of a big semi semi-elliptical defect 100/14 mm, the bearing capability of the pipe deteriorates rapidly with an increase in the internal pressure, it is controlled by the defect, and the critical conditions of failure are achieved much sooner. It should be noted that although the present analysis assumes linear elastic behavior, the Von Mises contours at higher pressures suggest localized plastic deformation. A more accurate prediction of stress redistribution near the crack tip could be obtained by incorporating an elasto-plastic material model, which will be considered in future studies.

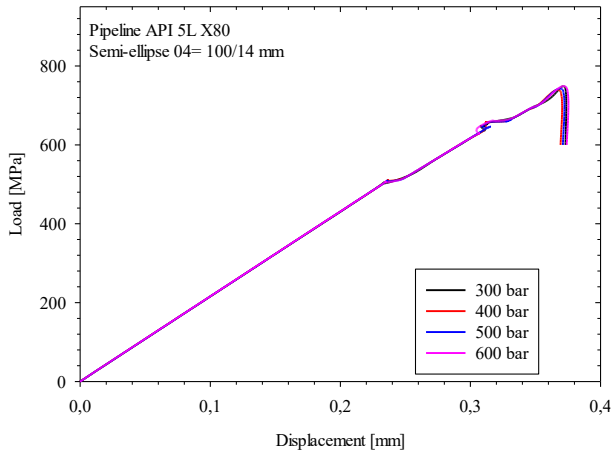

Figure11. load-displacement curve for defect a/t=0.88.

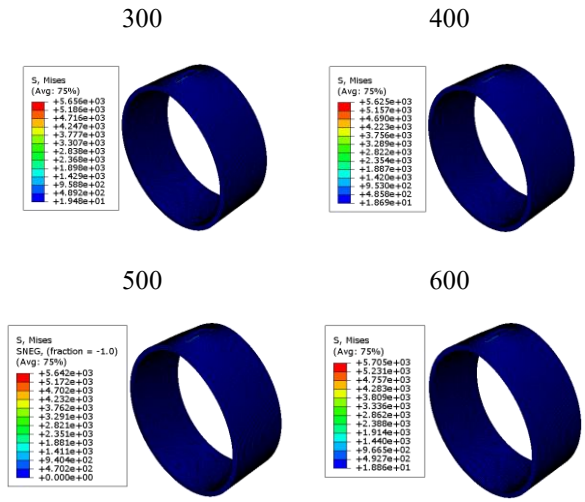

Figure 12. Von misses stress distribution at different pressure for defect a/t=0.88.

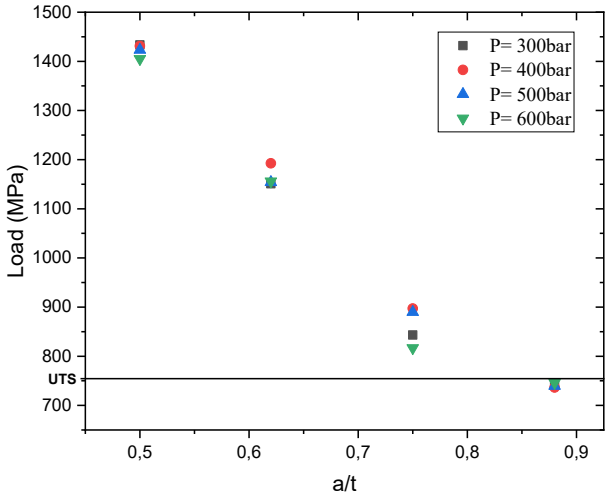

Figure 13. Variation of Pipe Resistance Capacity with Crack Depth Ratio (a/t) Compared to Ultimate Stress Limit.

Figure 12 presents the distribution of von Mises stresses around a semi elliptical defect with dimensions 100/14 mm for rising internal pressures of 300, 400, 500, and 600 bar. It gives evidence for a rather strongly localized stress field close to the crack tips. The higher the internal pressure, the higher the von Mises stress. At an internal pressure value of 300 bars, the stress concentrations are to be seen; however, these stresses remain concentrated in the close vicinity of the crack. Whereas for pressures of 400 and 500 bar, the distribution of stress has expanded and von Mises stresses approach a critical value along defect edges, well into the surrounding material of the pipe. In this case, at 600 bar it is seen from the figure that von Mises stress has reached a peak and furthers away from crack tips with broadened zones of high plastic deformation, particularly along the major axis of the defect. This increased distribution of stress shows how the internal pressure increases the presence of stress around the defect, hence weakening the pipe. It is underlined that the material near the crack is very susceptible to yielding and possible fracture, and the critical effect that a large semi-elliptical defect would have on the pipe's structural integrity due to high internal pressures is 100/14 mm in dimension.

Figure 13 represents a pipe's resistance capacity in terms of the crack size ratio (a/t), illustrating how the pipe's structural integrity diminishes as the crack becomes deeper. When the crack size ratio varies between 0.5 to 0.8 can be seen that the resistance capacity curve lies above the ultimate stress of the material; these results are not physically meaningful, as they imply that the pipe can withstand stresses beyond the material's inherent strength. Such a region is typically disregarded in practice, as it indicates an overestimation of the pipe's capacity. This behavior arises primarily from modeling assumptions in which plasticity and fracture effects were not included, combined with numerical artifacts inherent to XFEM interpolation near the crack tip

At the pressure P= 600 bar can be seen that the resistance capacity equals the ultimate stress at the crack size ratio a/t=0.9, which marks a transition point where the crack is small enough that the pipe behaves similarly to an uncracked component, potentially representing the maximum allowable flaw size under ultimate loading. However, the most critical and realistic interpretation lies in the region where the resistance capacity falls below the ultimate stress, as seen at the crack size ratio in the case of 300bar-500bar. This indicates that the presence of the crack significantly reduces the pipe's ability to withstand loads, and as the crack depth increases, the pipe becomes more susceptible to failure at stress levels lower than the ultimate. The intersection

between the curve and the ultimate stress line defines the critical crack size, beyond which failure is expected before reaching the material's full strength. This interpretation is essential for assessing the safety margin and determining acceptable defect sizes under operational loading conditions.

5.2 Failure assessment diagram

To construct the Failure Assessment Diagram (FAD), two key parameters must be calculated: the load ratio Lr and the fracture ratio Kr. The load ratio Lr is defined as the ratio between the gross stress σg and the flow stress σc, given by Lr=σg/σc. The reference stress typically accounts for the presence of the crack and is determined through analytical or numerical methods based on the defect geometry and loading conditions. The fracture ratio Kr is calculated as the ratio of the applied stress intensity factor (KI) to the material's fracture toughness (KIC), expressed as Kr=KI/KIC. The fracture toughness of the pipeline steel (X80) was taken as K_IC = 237.99 MPa√m. This value was used for normalizing the stress intensity factors in the Failure Assessment Diagram (FAD)." The stress intensity factor KI reflects the severity of the stress field near the crack tip under the applied load. Once the pairs of (Lr, Kr) values are obtained for various loading conditions or crack sizes, they are plotted to form the FAD. The table 3 represent these key parameters.

Table 3: Key parameters of FAD diagram.

a/t	**0.5**	**0.62**	**0.75**	**0.88**
$\mathbf{K_{Imax}}$	66.28	93.50	120.8	155
Kr	0,27849	0,39286	0,50756	0,65126
$\boldsymbol{\sigma_g = \frac{Pr}{t-a}}$	417,53	559,06	845,76	1736,05
$\boldsymbol{\sigma_c = (\sigma_y + \sigma_{ul})/2}$	697	697	697	697
$\mathbf{Lr = \frac{\sigma_g}{\sigma_c}}$	0,59904	0,80209	1,21343	1,30075

The FAD (Failure Assessment Diagram) represent in figure 14 results for the four defect dimensions (a/t ratios) under internal pressure of 30 MPa show a clear distinction between safe and failure conditions. The cases with a/t = 0.50 and a/t = 0.62 fall within the safety zone of the diagram, indicating that the pipe retains sufficient structural integrity and can withstand the applied pressure without critical failure. On the other hand, the cases with a/t = 0.75 and a/t = 0.88 are located within the failure zone, suggesting that cracks of this depth significantly reduce the pipe's load-carrying capacity, leading to instability or fracture under the same loading conditions. This behavior is consistent with expectations: as the relative crack depth (a/t) increases, the remaining ligament thickness decreases, causing a higher stress concentration and reducing the material's resistance to failure. These results indicate that for circumferential semi-elliptical cracks, a/t ratios approaching 0.75 correspond to a significant reduction in load-bearing capacity, marking the transition into the failure zone of the FAD assessment. From an engineering perspective, this implies that pipelines with defects deeper than ~75% of the wall thickness should be prioritized for immediate inspection, repair, or replacement, as their residual strength is severely compromised. This finding is consistent with industry acceptance criteria, such as those in API 579 and ASME B31G, which generally consider defects exceeding 70–80% of the wall thickness to be unacceptable for continued operation.

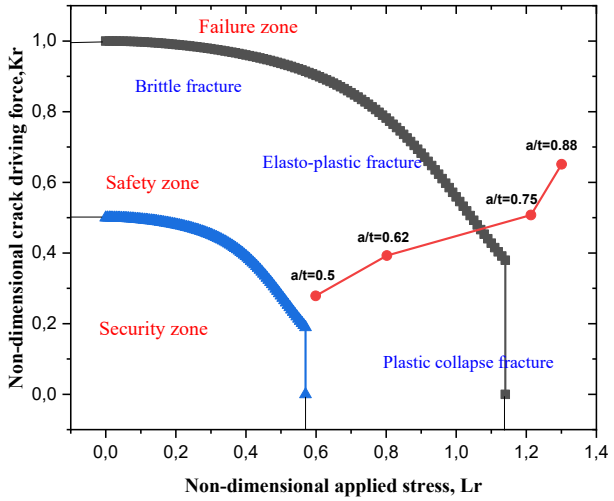

Figure 14. Failure Assessment diagramme for P=30MPa at different defect ratio (a/t).

6. Conclusions

This study demonstrates the pronounced influence of internal pressure on the bearing capacity of pipelines containing semi-elliptical cracks. As the internal pressure increases from 300 to 600 bar, the bearing capacity decreases significantly. This reduction is

attributed to elevated stress concentrations at the crack tips, which intensify the hoop stress and increase the Stress Intensity Factor (SIF), thereby accelerating crack propagation. At higher pressures, the combined effects of crack nucleation and growth further diminish the effective cross-sectional area, ultimately reducing the pipeline's load-bearing capacity.

In All cases, the resistance capacity decreases by approximately 85% as the defect depth ratio a/ta/ta/t increases from 0.50 to 0.62, by about 75% when the ratio increases from 0.62 to 0.75**,** and by nearly **77**% as the ratio further increases from 0.75 to 0.88. The rapid reduction of resistance capacity with increasing a/ta/ta/t is caused by the combined effect of reduced wall thickness available to carry loads and the nonlinear growth of stress concentration at the crack tip**,** which makes deeper cracks far more dangerous than shallow ones.

The study further demonstrated that defect size, expressed as the crack depth-to-thickness ratio (a/t), has a pronounced influence on stress distribution and the residual strength of the pipeline under identical loading conditions. As the a/t ratio increases, the resistance capacity of the pipe decreases, rendering it more susceptible to failure at lower stress levels. The critical crack size is identified at the point where the resistance curve intersects the ultimate stress line, beyond which failure is expected to occur before the material reaches its full strength. Regions in which the predicted resistance exceeds the ultimate stress are considered non-physical and are excluded from safe and realistic defect assessments. Under an internal pressure of 30 MPa, pipes with a/t ratios of 0.50 and 0.62 remain within the safety zone, preserving sufficient structural integrity. In contrast, at a/t ratios of 0.75 and 0.80, the pipe transitions into the failure zone, indicating a substantial reduction in load-bearing capacity and an elevated risk of instability or fracture.

The results highlight the critical influence of crack depth ratio (a/t) and internal pressure on pipeline integrity. For safe operation, defect depths beyond [insert your result threshold] should be considered unacceptable. The findings suggest that pipelines with smaller surface cracks may remain stable under moderate pressures, but deeper semi-elliptical defects significantly reduce load-bearing capacity. This has direct implications for setting allowable a/t limits in fitness-for-service assessments. The study supports the need for more frequent inspections in pipelines operating under high internal pressures or with known external surface defects.

The analysis was based on numerical modeling only, without experimental validation. Material properties were assumed to be homogeneous and isotropic, neglecting microstructural effects and residual stresses. Although semi-elliptical cracks were modeled in 3D, certain simplifications were applied to boundary conditions and loading scenarios.

Future work should focus on incorporating experimental data to validate XFEM predictions.

Extending the study to consider hydrogen embrittlement, corrosion-assisted cracking, and temperature effects. Developing probabilistic approaches to account for variability in material toughness and defect geometry.

References

[1] H. A. Kishawy and H. A. Gabbar, "Review of pipeline integrity management practices," International Journal of Pressure Vessels and Piping, vol. 87, no. 7, pp. 373–380, 2010. https://doi.org/10.1016/j.ijpvp.2010.04.003

[2] K. Yuan, K. Dong, and Q. Fang, "General point load weight function of stress intensity factors for external circumferential surface cracks in pipes," Ocean Engineering, vol. 308, p. 118263, 2024. https://doi.org/10.1016/j.oceaneng.2024.118263

[3] ULLAH, Niamat, AHMED, Zahoor, et KIM, Jong-Myon. Pipeline leakage detection using acoustic emission and machine learning algorithms. Sensors, vol. 23, p. 3226. 2023. https://doi.org/10.3390/s23063226

[4] FENG, Qingshan, LI, Rui, NIE, Baohua, et al. Literature review: Theory and application of in-line inspection technologies for oil and gas pipeline girth weld defection. Sensors, vol. 17, p. 50, 2016. https://doi.org/10.3390/s17010050

[5] QIN, Guojin, CHENG, Y. Frank, et ZHANG, Peng. Finite element modeling of corrosion defect growth and failure pressure prediction of pipelines. International journal of pressure vessels and piping, vol. 194, p. 104509. 2021. https://doi.org/10.1016/j.ijpvp.2021.104509

[6] TANG, Hai, LI, Chengpu, XU, Meng, et al. Fatigue crack growth behavior of X80 pipeline girth welded joints in natural gas/mixed hydrogen environment: Experimental and numerical investigations. Corrosion Science, Vol 252 , p. 112959. 2025. https://doi.org/10.1016/j.corsci.2025.112959

[7] MOHTADI-BONAB, M. A. Effects of different parameters on initiation and propagation of stress corrosion cracks in pipeline steels: a review. Metals, vol. 9, no 5, p. 590, 2019. https://doi.org/10.3390/met9050590

[8] SUN, Jialin et CHENG, Y. Frank. Assessment by finite element modeling of the interaction of multiple corrosion defects and the effect on failure pressure of corroded pipelines. Engineering Structures, 2018, vol. 165, p. 278-286. https://doi.org/10.1016/j.engstruct.2018.03.040

[9] YU, Mengshan, XING, Xiao, ZHANG, Hao, et al. Corrosion fatigue crack growth behavior of pipeline steel under underload-type variable amplitude loading schemes. Acta Materialia, vol. 96, p. 159-169,2015. https://doi.org/10.1016/j.actamat.2015.05.049

[10] MONTASSIR, S., YAKOUBI, K., MOUSTABCHIR, H., et al. Analysis of crack behaviour in pipeline system using FAD diagram based on numerical simulation under XFEM. Applied Sciences, vol. 10, no 17, p. 6129, 2020. https://doi.org/10.3390/app10176129

[11] BARTAULA, Durlabh, LI, Yong, KODURU, Smitha, et al. Simulation of fatigue crack growth using XFEM. In : Pressure Vessels and Piping Conference. American Society of Mechanical Engineers, Vol 3 p. T03A046. 2020. https://doi.org/10.1115/PVP2020-21637

[12] Z. Guo, H. Huang, and J. Chen, "Fatigue crack growth behavior of pipeline steel under cyclic loading with different frequencies," Fatigue & Fracture of Engineering Materials & Structures, vol. 41, no. 6, pp. 1308–1320, 2018.

[13] C. Arroussi, A. Belalia, and M. H. Meliani, "Numerical analyses on limit load of X60 pipe elbow in different internal corrosion-damaged positions under combined internal pressure and in-plan bending moment," International Journal on Interactive Design and Manufacturing (IJIDeM), vol. 18, no. 7, pp. 4661–4671, 2024. https://doi.org/10.1007/s12008-024-01736-y

[14] C. Arroussi, B. G. N. Muthanna, I. Chekalil, Z. Driss, and H. F. Isleem, "Predicting damage in steel pipe elbow under combined pressure and bending using X-FEM," International Journal of Steel Structures, pp. 1–10, 2025. https://doi.org/10.1007/s13296-025-00953-9

[15] C. Arroussi, A. Belalia, and M. H. Meliani, "Temperature effects on the resistance capacity of API X60 pipe elbow under bending moment using X-FEM method," Journal of Mechanical Science and Technology, vol. 38, no. 2, pp. 661–669, 2024. https://doi.org/10.1007/s12206-024-0114-0

[16] C. Arroussi, A. Belalia, and M. H. Meliani, "Effects of composite and metallic patch on the limit load of pressurized steel pipes elbow with internal defects under opening bending moment," Structural Monitoring and Maintenance, vol. 10, no. 3, pp. 221–242, 2023. https://doi.org/10.12989/smm.2023.10.3.221

[17] T. Belytschko, N. Moës, and S. Usui, "Arbitrary discontinuities in finite elements," International Journal for Numerical Methods in Engineering, vol. 50, no. 4, pp. 993–1013, 2009. https://doi.org/10.1002/1097-0207(20010210)50:4<993::AID-NME164>3.0.CO;2-M

[18] T. Belytschko and T. Black, "Elastic crack growth in finite elements with minimal remeshing," International Journal for Numerical Methods in Engineering, vol. 58, no. 2, pp. 187–209, 2003. https://doi.org/10.1002/(SICI)10970207(19990620)45:5<601::AID-NME598>3.0.CO;2-S

[19] N. Moës, J. Dolbow, and T. Belytschko, "A finite element method for crack growth without remeshing," International Journal for Numerical Methods in Engineering, vol. 46, no. 1, pp. 131–150, 1999. https://doi.org/10.1002/(SICI)10970207(19990910)46:1<131::AID-NME726>3.0.CO;2-J

[20] WU, Liang, ZHANG, Li Xing, et GUO, Ya Kun. A review of the extended finite element for fracture analysis of structures. Applied Mechanics and Materials, vol. 444, p. 96-102, 2014. https://doi.org/10.4028/www.scientific.net/AMM.444-445.96

[21] KANTH, Showkat Ahmad, HARMAIN, G. A., et JAMEEL, Azher. Investigation of fatigue crack growth in engineering components containing different types of material irregularities by XFEM. Mechanics of Advanced Materials and Structures, vol. 29, p. 3570-3587, 2022, https://doi.org/10.1080/15376494.2021.1907003

[22] YU, Mengshan, XING, Xiao, ZHANG, Hao, et al. Corrosion fatigue crack growth behavior of pipeline steel under underload-type variable amplitude loading schemes. Acta Materialia, vol. 96, p. 159-169. 2015. https://doi.org/10.1016/j.actamat.2015.05.049

[23] P. Zhao, J. Shuai, Z. Lv, and K. Xu, "Strain response of API 5L X80 pipeline subjected to indentation," Applied Ocean Research, vol. 94, p. 101991, 2020. https://doi.org/10.1016/j.apor.2019.101991